Phase dependence of high-order above-threshold ionization in asymmetric molecules

Qing Liao, Peixiang Lu,* Pengfei Lan, Wei Cao, and Yuhua Li
Wuhan National Laboratory for Optoelectronics, Huazhong University of Science and Technology, Wuhan 430074, People's Republic of China

(Received 25 September 2007; published 23 January 2008)

The high-order above-threshold ionization (ATI) by a few-cycle pulse in asymmetric molecules has been investigated by solving the time-dependent Schrödinger equation. The resulting high-energy ATI spectra are very sensitive to the laser's carrier-envelope phase (CEP) and analyzed in terms of the classical model. The left-right asymmetry of ATI yields of asymmetric molecules for high energies is different from that of atoms, resulting from the existence of an asymmetric potential well, and is explained by studying the molecules in the presence of a static electric field. The asymmetry for asymmetric molecules is expected to be used for measuring the CEP more accurately than for atoms.

DOI: 10.1103/PhysRevA.77.013408 PACS number(s): 32.80.Rm, 42.50.Hz, 42.65.Re

I. INTRODUCTION

Over the past two decades, intense laser interactions with atoms and molecules have been studied extensively. One of the major strong field processes, above-threshold ionization (ATI) [1], can be described by the classical rescattering model [2,3] qualitatively. The low-energy part of ATI spectra corresponds to photoelectrons that are emitted without further interaction with the core, while the high-energy part of ATI spectra to photoelectrons that can scatter elastically from the core after they are driven back by the laser field and are further accelerated by the field.

Recently, intense ultrashort laser pulses with durations as short as a few optical cycles have been generated and are available as research tools [4–9]. Such few-cycle pulses (FCPs) have been used for generating coherent soft x rays [10] and attosecond pulses [11] and have a high potential for applications in many other fields such as coherent control of molecular dynamics. All these processes depend on the time variation of the laser field and thus on the phase of the carrier frequency with respect to the envelope, the so-called carrier-envelope phase (CEP). Therefore, measuring and precisely stabilizing the CEP is crucially important in view of many possible applications. The left-right asymmetry of ATI yields of atoms has been first shown in a "stereo-ATI" experiment with circularly polarized few-cycle non-phase-stable laser pulses [12]. The asymmetry is sensitive to the CEP and particularly pronounced for high energies. In experiment, the left-right asymmetry of high-energy photoelectrons has been used to measure and stabilize the CEP [13] and to measure the Gouy phase shift [14]. While these experiments demonstrated how the results vary with the CEP of the FCPs, the determination of its actual value has to rely on the prediction of theoretical calculations. The dependence of the asymmetry of ATI yields on the CEP of FCPs for atoms has been studied theoretically in many papers recently [15–18]. The dependence of the angular distribution of photoelectrons on the CEP has been investigated for symmetric molecules exposed to a circularly polarized FCP, and steering of low-energy photoelectrons in space was suggested by controlling the CEP [19].

For asymmetric molecules, the electron cloud is localized predominantly on the most electronegative ion and thus the left-right asymmetry of high-energy photoelectrons is expected to be different from that for atoms. As the simplest heteronuclear asymmetric molecular ion, HeH^{2+} has been the subject of many experimental and theoretical works [20–22]. The phase dependence of enhanced ionization has been studied for HeH^{2+} by a linearly polarized FCP and explained by studying the molecule in the presence of a static electric field oriented parallel and antiparallel to the PDM [23]. In this paper, we investigate the phase dependence of high-order ATI spectra of asymmetric molecules driven by a FCP linearly polarized along the internuclear axis by solving the one-dimensional time-dependent Schrödinger equation (TDSE). The resulting high-energy ATI spectra exhibit the characteristic left-right asymmetry and large-scale interference patterns. The cutoff energies of high-energy photoelectrons are very sensitive to the CEP. The left-right asymmetry is much stronger for the CEP ranging from π to 2π than for the CEP ranging from 0 to π, which is different from that of atoms. Simulations of asymmetric double potential wells in a static electric field provides an explanation for this effect. The phase dependence of the asymmetry and the cutoff energies of high-energy ATI yields implies that steering the emission of high-energy photoelectrons in space and their energy range can be achieved by controlling the CEP. The paper is organized in the following manner. Section II describes the simulation model. In Sec. III, we present our results with discussions and give classical analyses for the results. Finally, we shall summarize the paper in Sec. IV. Atomic units are used throughout the paper unless otherwise stated.

II. SIMULATION MODEL

The one-dimensional TDSE for heteronuclear diatomic molecules driven by a FCP linearly polarized along the internuclear axis has the following form:

$$i\frac{\partial\Psi(x,t)}{\partial t}=\left[-\frac{1}{2}\frac{\partial^2}{\partial x^2}+V(x)+xE(t)\right]\Psi(x,t), \qquad (1)$$

where

*Corresponding author. lupeixiang@mail.hust.edu.cn

$$V(x) = -\frac{Z_1}{\sqrt{1+(x-R/2)^2}} - \frac{Z_2}{\sqrt{1+(x+R/2)^2}} \tag{2}$$

is a soft-Coulomb potential used to describe the attractions of two nuclei to the electron, where R is the internuclear distance, Z_1 and Z_2 are the electric charges of the two nuclei, which are considered to be fixed at $\pm R/2$, respectively. Calculations with the two-center soft-Coulomb potential are not expected to reproduce experiments on real diatomic molecular ions, because ionization of real diatomic molecular ions is dominated by charge resonance enhanced ionization at internuclear separations much larger than the equilibrium bond length [24]. The model is, however, suitable to describe many features of the ionization of neutral molecules which usually occurs near the ground-state geometry [25]. $E(t)$ is the laser electric field.

We use a wave-function splitting technique [18,26] to calculate the ATI spectra. The electron wave function $\Psi(x,t)$ is split into two parts at a given time t_i:

$$\Psi(x,t_i) = \Psi_I(x,t_i) + \Psi_{II}(x,t_i) = \Psi(x,t_i)[1 - F_s(R_c)] + \Psi(x,t_i)F_s(R_c). \tag{3}$$

Here, $F_s(R_c) = 1/(1+e^{(|x|-R_c)/\Delta})$ is a split function that separates the whole space into the inner $(0 \to R_c)$ and outer $(R_c \to R_{\max})$ regions smoothly. Here Δ represents the width of the crossover region. $\Psi_I(x,t_i)$ represents the wave function in the inner region, and $\Psi_{II}(x,t_i)$ stands for the wave function in the outer region. The calculation scheme relies on the assumption that in the outer region the Coulomb potential can be neglected. The exact time evolution of $\Psi_I(x,t_i)$ is evaluated using the split-operator spectral method [27]. The Fourier transform $\varphi(p,t_i)$ of $\Psi_{II}(x,t_i)$ can be propagated to some final time $t_f \geq T$ using the exact formula

$$\varphi'(p,t_i) = \exp\left(-i\int_{t_i}^{t_f} \frac{1}{2}[p + A(t')]^2 dt'\right)\varphi(p,t_i), \tag{4}$$

where

$$A(t_i) = -\int_{t_i}^{t_f} E(t)dt, \tag{5}$$

and

$$\varphi(p,t_i) = (2\pi)^{-1/2}\int \Psi_{II}(x,t_i)\exp\{-i[p + A(t_i)]x\}dx. \tag{6}$$

The momentum wave function is propagated by Eq. (4) so that there is no boundary problem any more. The ATI spectra of the ionized electrons in the left and right sides are calculated according to the formulas

$$\frac{dP_L(E)}{dE} = \frac{1}{p(E)}\left|\sum_i \varphi'_-(p,t_i)\right|^2, \tag{7}$$

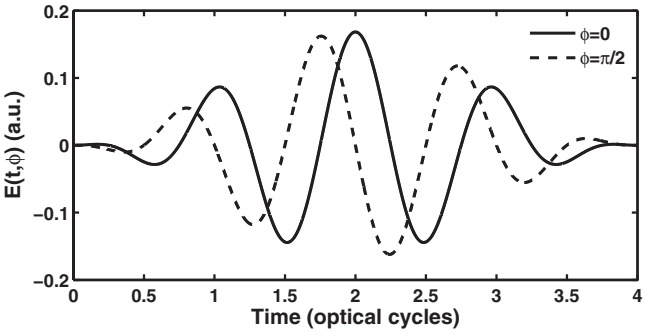

FIG. 1. Electric field $E(t,\phi)$ as a function of time in optical cycles for CEPs $\phi=0$ (solid line) and $\phi=\pi/2$ (dashed line). The peak intensity is $I=1\times10^{15}$ W/cm^2.

$$\frac{dP_R(E)}{dE} = \frac{1}{p(E)}\left|\sum_i \varphi'_+(p,t_i)\right|^2, \tag{8}$$

where $\varphi'_-(\varphi'_+)$ are wave functions corresponding to the electron moving in the negative (positive) direction along the x axis, i.e., the left (right) side, respectively, and $p(E)=\sqrt{2E}$.

In our simulation, the internuclear distance $R=4$ a.u., $Z_1=1$ a.u., $Z_2=2$ a.u. The few-cycle laser pulse has a sine squared envelope with a laser frequency $\omega=0.057$ a.u. ($\lambda=800$ nm) and a peak intensity $I=1\times10^{15}$ W/cm^2. The electron ponderomotive radius and ponderomotive energy are $\alpha_0=51.8$ a.u. and $U_p=2.18$ a.u., respectively. The total pulse duration T_p is four optical cycles. Figure 1 shows the electric field of the laser:

$$E(t,\phi) = E_0 \sin^2(\omega t/8)\cos[\omega(t - T_p/2) + \phi] \tag{9}$$

for the CEPs $\phi=0$ and $\phi=\pi/2$. We choose $R_{\max}=450$ a.u., $R_c=300$ a.u., and $\Delta=6$, which gives a crossover region width of $\sim$80 a.u.. The splitting of the wave function is applied 30 times per optical cycle. Note that the values of all parameters used in our simulation satisfy the physical conditions [26] for the validity of Eqs. (7) and (8). After the end of the pulse, the wave function is allowed to propagate without laser field for an additional time of four optical cycles in order to collect all photoelectrons with energies above $0.05U_p$. The initial wave function for time propagation is chosen to be the field-free ground state, which is obtained by propagation in imaginary time.

III. RESULTS AND DISCUSSIONS

Figure 2 shows our simulated ATI spectra as a function of the CEP. In the low-energy region (below $\sim 2U_p$), the ATI yields of the left are larger than those of the right and the ATI spectra are not sensitive to the CEP. In the high-energy region (above $\sim 4U_p$), the ATI spectra exhibit obvious plateaus and large-scale interference patterns and the ATI yields are very sensitive to the CEP. The cutoff energy of the plateau in the high-energy ATI spectrum of the left labeled with L_1 is about $\sim 6.3U_p$ for the CEP $\phi=0$. As the CEP increases up to π, the cutoff energy of L_1 increases up to $\sim 10.2U_p$, but the yields of L_1 decreases quickly. As the CEP increases further,

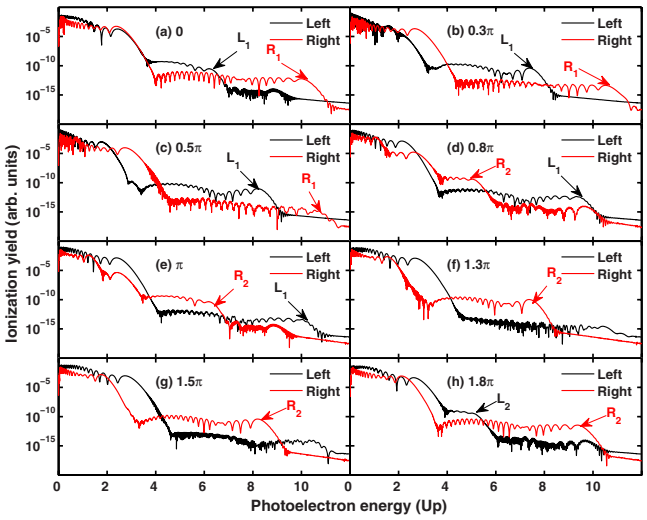

FIG. 2. (Color online) Ionization yields of asymmetric molecules to the left and right sides as a function of the CEP. Plots (a)–(g) are for CEPs $\phi=0$, 0.3π, 0.5π, 0.8π, π, 1.3π, 1.5π, 1.8π, respectively.

the yields of L_1 disappears to the background. A new plateau of the left with cutoff energy $\sim 4U_p$, which is not clear, appears for the CEP $\phi=1.5\pi$. The cutoff energy of this plateau labeled with L_2 in Fig. 2(h) is extended to $\sim 5U_p$. When the CEP increases further, plateau L_2 is obviously expected to replace the role of plateau L_1. The high-energy ATI spectra of the right are similar to those of the left when their corresponding CEPs have a difference of π, but the yields in the former are higher than those in the latter. This is different from the high-energy ATI spectra of atoms of the left and right which are identical when their corresponding CEPs have a difference of π. This difference will be explained below.

The cutoff energies of the plateaus in high-energy ATI spectra are very sensitive to the CEP. Figure 3 shows the cutoff energies of the plateaus as functions of the CEP. When the CEP ranges from $-0.5\pi+2n\pi$ to $0.5\pi+2n\pi$ (n is an integer), the plateau of the left with cutoff energy ranging from $\sim 4U_p$ to $\sim 8.3U_p$ has relative high yields, while the

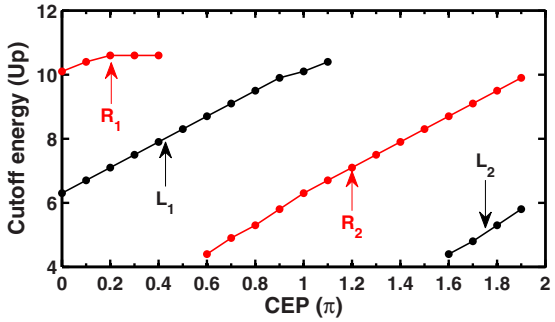

FIG. 3. (Color online) The cutoff energies of the plateaus in the high-energy ATI spectra as functions of the CEP. The black circles represent the cutoff energies of plateaus L_1 and L_2, respectively, and the red circles represent the cutoff energies of plateaus R_1 and R_2, respectively. The line is drawn to guide the eye.

plateau of the right with cutoff energy ranging from $\sim 4U_p$ to $\sim 8.3U_p$ has relative high yields when the CEP ranges from $0.5\pi+2n\pi$ to $1.5\pi+2n\pi$. The simple linear relation between the cutoff energies of the plateaus and the CEP may be used as an efficient tool for measuring the CEP of FCPs. In experiment, it will be better for atoms since this feature also holds for atoms obviously. Next, we intend to give a one-dimension classical analysis for the cutoff energies in high-energy ATI spectra in terms of the classical rescattering model generalized to FCPs [28–30].

Suppose the electron is "born" at the origin with zero velocity at some time $0 \le t_0 \le T_p$ in the presence of only the laser field. Solving Newton's equation of motion $\dot{v}=-E(t)$, we obtain the electron momentum at some arbitrary later time $t > t_0$:

$$v(t) = A(t) - A(t_0). \tag{10}$$

If at some time $t_1 > t_0$, the electron returns to the origin, i.e.,

$$r(t_1) = \int_{t_0}^{t_1} dt A(t) - A(t_0)(t_1 - t_0) = 0, \tag{11}$$

it may elastically rescatter off its parent ion. Thereafter, the electron moves in the laser field only, up to the time T_p, when the laser field is switched off. The final electron energy is

$$E_p = \frac{1}{2}p^2 = E_p(t_0), \tag{12}$$

with

$$p \equiv A(T_p) - 2A(t_1) + A(t_0). \tag{13}$$

High-energy photoelectrons returning to the parent ion can be created only in short time intervals close to peaks of the electric field of the laser pulse. The probability that they tunnel through the potential barrier depends exponentially on the field strength at the ionization time t_0 and as FCPs are involved it is likely only for those very few optical half cycles close to the pulse maximum [13]. After the rescattering time, the field must still be sufficiently strong to accelerate them to high energies. The solutions of the classical model are presented in Figs. 4(a)–4(d) for the cases of Figs. 2(a)–2(d), respectively. The final photoelectron energy $E_p(t_0)$ is shown as a function of the ionization time t_0. Evidently, the rescattering photoelectrons emitted to the left (right) are created in short time intervals close to peaks of the electric field when the direction of the field is positive(negative). Figure 4 exhibits the solutions that may contribute significantly to the plateaus. We denote these solutions by the ionization time that leads to the cutoff (highest) energy $E_p(t_0)$, that is, by the pair, t_0[optical cycle], $E_p(t_0)[U_p]$. With this notation, the two pairs of the left for the CEP $\phi=0$, as shown in Fig. 4(a), are $L_1'=(2.05,6)$, $L_2'=(0.99,8.7)$ and the two pairs of the right are $R_1'=(1.53,9.9)$, $R_2'=(2.58,1.6)$. Obviously, L_1' and R_1' are associated with plateau L_1' and plateau R_1 of Fig. 2(a), respectively. L_2' corresponds to the plateau of the left with cutoff energy $\sim 9U_p$ which is not very clear in Fig. 2(a). R_2' cannot be identified in Fig. 2(a) because its cutoff $1.6U_p$ lies in the low-energy region which is domi-

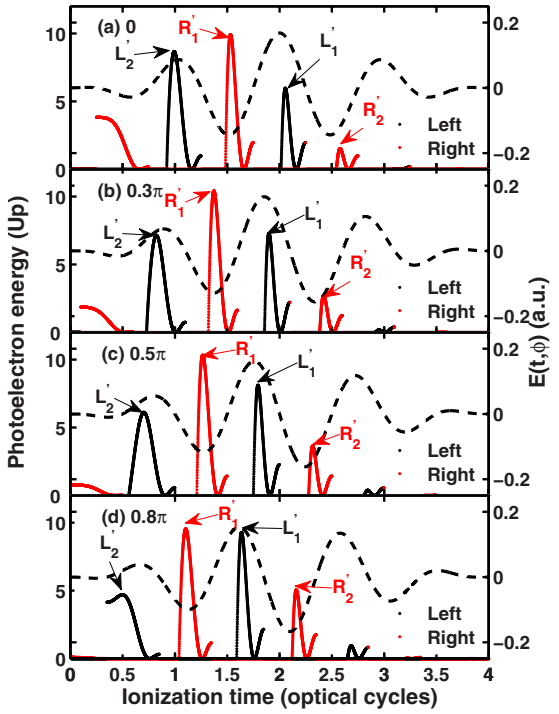

FIG. 4. (Color online) Solutions of the classical rescattering model for the parameters of Figs. 2(a)–2(d). The black (red) dots specify the final energy of rescattered photoelectrons emitted to the left (right) side as a function of the ionization time. The dashed curve indicates the electric field $E(t,\phi)$ with the scale given on the right-hand ordinate.

nated by the direct electrons. The two solutions of the pair L_1' (or R_1') for some given energy beat against each other and thus result in the large-scale interference pattern as shown in Fig. 2(a). In quantum theory, the large-scale interference pattern is explained as the superposition of two quantum orbits, the so-called "long" and "short" orbits [31]. The large-scale interference pattern essentially reveals subtle details of the ionization dynamics deep down to a time scale of a small fraction of the optical cycle, i.e., the attosecond time scale. As the CEP increases, the cutoffs of L_1' and R_2' increase because the field accelerating the electrons is stronger [see Figs. 4(b) and 4(c)].

When the CEP is changed, the ionization time and rescattering time, as well as the ionization probability, are also changed. Thus the photoelectron yields at highest energies depend strongly on the CEP. When the CEP is changed by π, the electric field essentially only changes sign. Accordingly, this only reverses the solutions of the left and right. The plateaus L_1, L_2, R_1, and R_2 essentially are dominated by rescattering electrons created only in short time intervals close to the two maximal peaks of the electric field near the maximum of the laser pulse.

The ratio of the total high-energy ($>6U_p$) ATI yields of the left and right is also plotted as a function of the CEP in Fig. 5. The high-energy ATI yields of the left are about two orders of magnitude higher than those of the right for the CEP ranging from 0 to π, while those of the right are about three orders of magnitude higher than those of the left for the

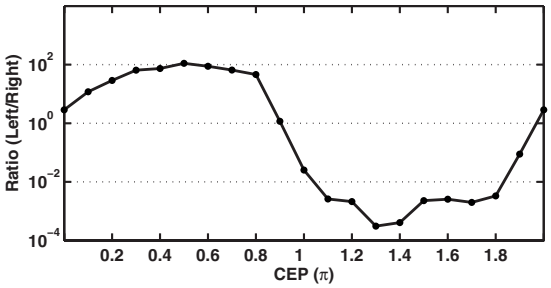

FIG. 5. Ratio of the total high-energy ($>6U_p$) ATI yields of left and right sides as a function of the CEP. Circles are the calculated data. The line is drawn to guide the eye.

CEP ranging from π to 2π. This is different from the case of atoms. For atoms, $\frac{P_L}{P_R}(\phi_1)=\frac{P_R}{P_L}(\phi_2)$ when their corresponding CEP difference $\phi_1-\phi_2=\pm\pi$, where $P_L(P_R)$ stands for the total high-energy yields of electrons emitted to the left (right) side. The asymmetry particularly pronounced for the CEP ranging from π to 2π for asymmetric molecules essentially results from the existence of an asymmetric potential well and can be explained as in Ref. [23].

The high-energy electrons are significantly created only in a short time interval so that the electric field can be considered to be constant. The electric field that significantly creates high-energy electrons emitted to the left side, denoted by $E_L(t,\phi)$, is parallel (positive direction) to the permanent dipole of the molecule (PDM), while the one that significantly creates high-energy electrons emitted to the right side, denoted by $E_R(t,\phi)$, is antiparallel (negative direction) to the PDM; see Fig. 4. The system's response to the FCP is similar to a response to a static field F oriented in the same direction as the electric field at the peaks of the pulse.

Figure 6 presents the schematic illustration of combined soft-Coulomb and static field potentials $V(x)+Fx$ for asymmetric molecules. Figures 6(b) and 6(c) correspond the case of Fig. 2(b) and Figs. 6(a) and 6(d) correspond the case of Fig. 2(f). For static field F antiparallel to PDM, the left potential well is lifted up, while the right potential well is dragged down. For static field F parallel to PDM, the left potential well is dragged down, while the right potential well is lifted up. The electron cloud of the ground state of asymmetric molecules is predominantly localized on the left well. Based on perturbation theory, the ground state energy of the molecule in a static field shifts by $|F|R/2$ approximately [32], where $R/2$ is the dipole moment. For the antiparallel orientation, the energy of the electron in the left well can be approximated by $E_A=E_g+|F|R/2$, where E_g is the ground state energy in the absence of external field, i.e., the electron energy increased by the action of the static field ($|F|R/2$). Similarly, for the parallel orientation, the energy of the electron in the left well can be approximately by $E_P=E_g-|F|R/2$, the energy of the electron is decreased by the action of the static field ($-|F|R/2$). For the antiparallel orientation [see Figs. 6(a) and 6(c)], the energy level of the electron in ground state is lifted up by the field and it tunnels through the thin internuclear potential barrier to reach the continuum to the right side. In contrast, for the parallel ori-

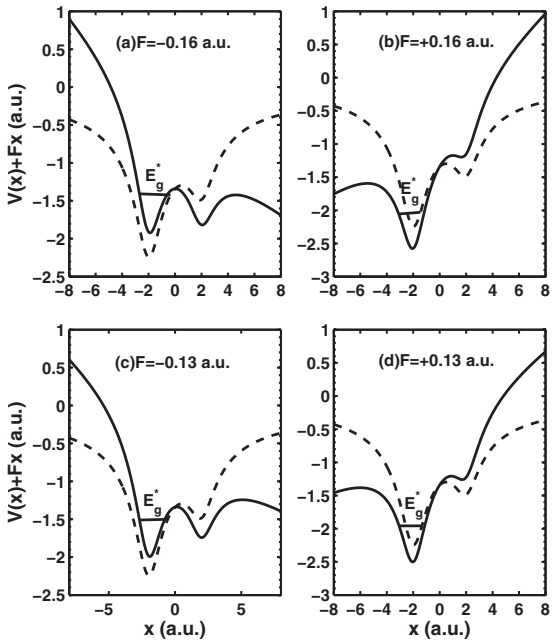

FIG. 6. Combined soft-Coulomb and static field potentials $V(x)+Fx$ for asymmetric molecules along the x axis. The static field in plots (b) and (c) corresponds the electric field of the pulse at the time $t=1.9$ and $t=1.37$ optical cycle, respectively, for the CEP $\phi=0.3\pi$, while the static field in plots (a) and (d) corresponds to the electric field of the pulse at the time $t=1.9$ and $t=1.37$ optical cycle, respectively, for the CEP $\phi=1.3\pi$. The soft-Coulomb potential $V(x)$ (dashed lines) is also plotted for comparison. Energies of the field-dressed ground state E_g^* are shown.

entation [see Figs. 6(b) and 6(d)], its energy level is dragged down by the field, so that it tunnels instead through a wider left potential barrier to ionize to the left side. As a result, $\frac{P_L}{P_R}(0.3\pi)<\frac{P_R}{P_L}(1.3\pi)$ for high-energy electrons. This explains the stronger left-right asymmetry of high-energy photoelectrons for the CEP ranging from π to 2π than for the CEP ranging from 0 to π.

The left-right asymmetry of high-energy ATI yields is expected to be stronger for asymmetric molecules than for atoms, which can be used for measuring the CEP of FCPs more accurately. The ground state and most electronic states of HeH^{2+} are repulsive because of the strong nuclei repulsion. In experiments, it is expected to use alkali-metal hydrides (LiH^+, etc.) and halogen compounds (HCl^+, etc.) which are stable molecular systems with asymmetric potentials and a single valence electron.

IV. SUMMARY

In summary, we have numerically investigated the high-order ATI spectra of heteronuclear asymmetric molecules driven by a linearly polarized FCP. The phase dependence of the high-energy ATI spectra on the CEP of the applied FCP implies that steering photoelectron emitting in space and its energy range can be achieved by controlling the CEP of FCPs, which may have applications in other fields such as photoelectron microscopy. The large-scale interference patterns in the high-energy ATI spectra can reveal subtle features in the ionization dynamics deep down into the attosecond time scale. The pronounced left-right asymmetry in the high-energy ATI spectra for the CEP ranging from π to 2π essentially results from the existence of an asymmetric potential well, which is expected to occur in any nonsymmetric polar molecule.

ACKNOWLEDGMENTS

This work was supported by the National Natural Science Foundation of China under Grants No. 10574050 and No. 10774054, the Specialized Research Fund for the Doctoral Program of Higher Education of China under Grant No. 20040487023, and the National Key Basic Research Special Foundation under Grant No. 2006CB806006.

[1] P. Agostini, F. Fabre, G. Mainfray, G. Petite, and N. K. Rahman, Phys. Rev. Lett. **42**, 1127 (1979).
[2] P. B. Corkum, Phys. Rev. Lett. **71**, 1994 (1993).
[3] G. G. Paulus, W. Becker, W. Nicklich, and H. Walther, J. Phys. B **27**, L703 (1994).
[4] T. Brabec and F. Krausz, Rev. Mod. Phys. **72**, 545 (2000).
[5] D. J. Jones, S. A. Diddams, J. K. Ranka, A. Stentz, R. S. Windeler, J. L. Hall, andS. T. Cundiff, Science **288**, 635 (2000).
[6] A. Apolonski, A. Poppe, G. Tempea, C. Spielmann, T. Udem, R. Holzwarth, T. W. Hansch, and F. Krausz, Phys. Rev. Lett. **85**, 740 (2000).
[7] M. Kakehata, H. Takada, Y. Kobayashi, Y. Fujihira, T. Homma, and H. Takahashi, Opt. Lett. **26**, 1436 (2001).
[8] A. Baltuška, T. Fuji, and T. Kobayashi, Phys. Rev. Lett. **88**, 133901 (2002).
[9] B. Schenkel, J. Biegert, U. Keller, C. Vozzi, M. Nisoli, G. Sansone, S. Stagira, S. De Silvestri, and O. Svelto, Opt. Lett. **28**, 1987 (2003).
[10] P. Villoresi, C. Ceccherini, L. Poletto, and G. Tondello, Phys. Rev. Lett. **85**, 2494 (2000).
[11] M. Hentschel *et al.*, Nature (London) **414**, 509 (2001).
[12] G. G. Paulus, F. Grasbon, H. Walther, P. Villoresi, M. Nisoli, S. Stagira, E. Priori, and S. De Silvestri, Nature (London) **414**, 182 (2001).
[13] G. G. Paulus, F. Lindner, H. Walther, A. Baltuska, E. Goulielmakis, M. Lezius, and F. Krausz, Phys. Rev. Lett. **91**, 253004 (2003).
[14] F. Lindner, G. G. Paulus, H. Walther, A. Baltuska, E. Goulielmakis, M. Lezius, and F. Krausz, Phys. Rev. Lett. **92**, 113001 (2004).
[15] D. B. Milošević, G. G. Paulus, and W. Becker, Phys. Rev. Lett. **89**, 193001 (2002).
[16] S. Chelkowski, A. D. Bandrauk, and A. Apolonski, Phys. Rev.

A **70**, 013815 (2004).
[17] C. Altucci, V. Tosa, R. Velotta, and C. H. Nam, Phys. Rev. A **70**, 065402 (2004).
[18] X. M. Tong, K. Hino, and N. Toshima, Phys. Rev. A **74**, 031405(R) (2006).
[19] S. X. Hu and L. A. Collins, Phys. Rev. A **73**, 023405 (2006).
[20] I. Ben-Itzhak, I. Gertner, O. Heber, and B. Rosner, Phys. Rev. Lett. **71**, 1347 (1993).
[21] I. Ben-Itzhak, J. P. Bouhnik, B. D. Esry, I. Gertner, O. Heber, and B. Rosner, Phys. Rev. A **54**, 474 (1996).
[22] P. Lan, P. Lu, W. Cao, Y. Li, and X. Wang, Phys. Rev. A **76**, 021801(R) (2007).
[23] G. L. Kamta and A. D. Bandrauk, Phys. Rev. Lett. **94**, 203003 (2005).
[24] T. Zuo and A. D. Bandrauk, Phys. Rev. A **52**, R2511 (1995); T. Seideman, M. Y. Ivanov, and P. B. Corkum, Phys. Rev. Lett. **75**, 2819 (1995).
[25] M. Lein, J. P. Marangos, and P. L. Knight, Phys. Rev. A **66**, 051404(R) (2002).
[26] S. Chelkowski, C. Foisy, and A. D. Bandrauk, Phys. Rev. A **57**, 1176 (1998).
[27] M. D. Feit,J. A. Fleck, Jr., and A. Steiger, J. Comput. Phys. **47**, 412 (1982).
[28] D. B. Milošević, G. G. Paulus, and W. Becker, Opt. Express **11**, 1418 (2003).
[29] D. B. Milošević, G. G. Paulus, and W. Becker, Laser Phys. Lett. **1**, 93 (2004).
[30] D. B. Milošević, G. G. Paulus, D. Bauer, and W. Becker, J. Phys. B **39**, R203 (2006).
[31] D. B. Milosevic, G. G. Paulus, and W. Becker, Phys. Rev. A **71**, 061404(R) (2005).
[32] Z. Mulyukov, M. Pont, and R. Shakeshaft, Phys. Rev. A **54**, 4299 (1996).